Transformation of Organic–Inorganic Hybrid Films Obtained by Molecular Layer Deposition to Photocatalytic Layers with Enhanced Activity

Sergey Ishchuk,[‡] Dereje Hailu Taffa,[‡] Ori Hazut, Niv Kaynan, and Roie Yerushalmi*

Institute of Chemistry and the Center for Nanoscience and Nanotechnology, The Hebrew University of Jerusalem, Edmond J Safra Campus, Givat Ram Jerusalem, 91904, Israel. [‡]Sergey Ishchuk and Dereje Hailu Taffa share equal contribution.

ABSTRACT

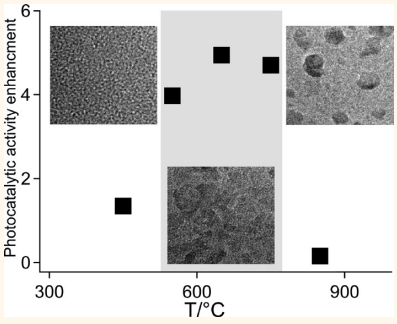

We present the transformation of organic–inorganic hybrid titanicone films formed by $TiCl_4$ as metal precursor and ethylene glycol (EG) using solvent-free MLD to highly active photocatalytic films. The photocatalytic activities of the films were investigated using hydroxyl-functionalized porphyrin as a spectroscopic marker. TEM imaging and electron diffraction, XPS, UV–vis spectroscopy, and spectroscopic ellipsometry were employed for structural and composition analyses of the films. The photocatalytic activity of Ti–EG films was investigated for different anneal temperatures and compared to TiO_2 films prepared by ALD using $TiCl_4$ as metal precursor and H_2O (TiO_2 films). Overall, our results indicate that the photocatalytic activity of the thermally annealed Ti–EG film is about 5-fold increased compared to that of the TiO_2 film prepared by ALD for optimal process conditions. The combined results indicate that the structural and photocatalytic properties can be assigned to three states: (I) amorphous state, intermediate dye loading, low photocatalytic activity, (II) intermediate film state with both crystalline and amorphous regions, high dye loading, high catalytic activity, and (III) highly crystalline film with low dye loading and low photocatalytic activity. The formation of photocatalytic nanotubes (NTs) is demonstrated using sacrificial Ge nanowires (NWs) scaffolds to yield Ti–EG NT structures with controllable wall thickness structures and enhanced dye loading capacity. Our results demonstrate the feasibility and high potential of MLD to form metal oxides with high photocatalytic activity.

KEYWORDS: nanowires · nanotubes · hybrid films · MLD · photocatalysis · TiO_2

Atomic layer deposition (ALD) is widely studied and applied for the controllable formation of highly conformal, pinhole free, molecularly impermeable metal oxide films.[1−3] Molecular layer deposition (MLD) is widely used for deposition of organic multilayered structures on different solid supports.[4−6] Recently, there is substantial progress in the development of MLD where the film is formed by metal precursor and an organic bifunctional molecular precursor, yielding organic–inorganic hybrid films with tunable properties.[7,8] Similar to metal oxide formation by ALD, MLD provides a solvent-free path for the formation of organic–inorganic hybrid thin film materials in a well-controlled manner.[9,10] In this regard aluminum, zinc, titanium, and zirconium metal containing precursors in combination with organic diols such as ethylene glycol, glycerol, and hydroquinone form the *metalcones* "alucone","zincone", "titanicone", and "zircone", respectively.[11,12] The MLD process of these organic–inorganic hybrid films yield atomically smooth and conformal films, and upon annealing a porous metal oxide framework is obtained.[9,11] Thus, both ALD and MLD methods are highly attractive for the formation of metal oxide (MO) thin films due to excellent uniformity, accurate control of film thickness, low deposition temperatures, and applicability to high aspect ratio structures, including at the nanometric scale.[13−18] The hybrid films formed by MLD can be prepared on macroscopic surfaces as well as on nanostructures such as nanoparticles, nanorods, and nanowires (NWs) with high geometrical aspect ratios. Among metal oxide materials accessible *via* the ALD and MLD approaches, TiO_2 is extensively studied due to broad potential technological applications including photocatalysis, conversion of light energy, energy storage, solar cells, and self-cleaning surfaces.[19−26] In addition to the vapor phase methods, TiO_2 may be prepared by a broad range of solution-based methods including sol–gel, hydrothermal, solvothermal, and evaporation-induced self-assembly methods.[27−32] These methods are versatile and flexible allowing for tuning of the film properties. However, thin film

* Address correspondence to roie.yerushalmi@mail.huji.ac.il.

Received for review May 29, 2012 and accepted July 6, 2012.

Published online July 07, 2012
10.1021/nn302370y

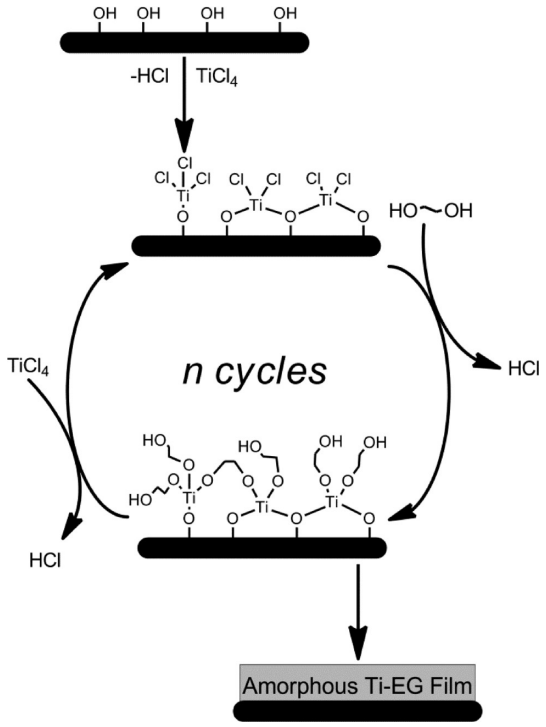

Scheme 1. Ti–EG MLD film formation with suggested surface reactions, binding modes, and coordination species. $TiCl_4$ and ethylene glycol are used as molecular precursors.

formation at the surface of high aspect ratio structures at the nanoscale with accurate control over film thickness in the range of a few nanometers is still challenging using solution-based methods. The MLD approach provides a promising path for overcoming some of the limitations encountered using conventional methods for the formation of catalytic metal oxide films for nanometric scale high aspect ratio structures since MLD combines the highly controlled, self-limiting characteristics of the ALD approach with the flexibility introduced by the organic molecular constituent. The organic parts of the MLD film can be retained as structural component of the film or utilized as a sacrificial component. Specifically, the formation of photocatalytic films by MLD where the oxide is a photocatalytic material, as in the case of TiO_2 is highly desired. To-date, however, neither the catalytic nor the photocatalytic properties of MLD films, has been demonstrated, including for titanicone films. Here we present the transformation of organic–inorganic hybrid films formed by solvent-free MLD to highly active photocatalytic films. We demonstrate the approach by using $TiCl_4$ as metal precursor and ethylene glycol as the organic component (Ti–EG film, Scheme 1).

RESULTS AND DISCUSSION

The Ti–EG MLD process is highly controlled, yielding uniform and conformal thin films on macroscopic surfaces (Figure 1a) as well as on nanometric structures (Figure 1d). The optimized process conditions are listed

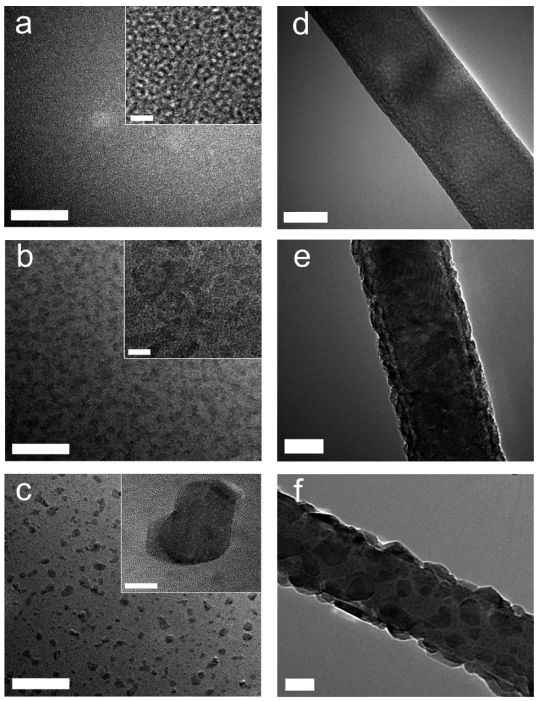

Figure 1. TEM images obtained for Ti–EG films formed on SiO_2 membrane (40 nm thick) following thermal anneal at (a) 250, (b) 650, and (c) 850 °C; Ti–EG films formed on Si NW demonstrating highly conformal and uniform film following thermal anneal at (d) 250, (e) 650, and (f) 850 °C. Scale bars (a–c) 200 nm, inset 10 nm; (d–f) 20 nm.

in Supporting Information, Table S1. Ellipsometric measurements show Ti–EG film thickness grow linearly with the MLD cycle with 4.5–6.0 Å thickness increase per $TiCl_4$/EG cycle at the temperature range studied, 100–120 °C. (Supporting Information, Figure S1). For $TiCl_4/H_2O$ the growth per cycle is 0.8 Å at 100 °C, in good agreement with previously reported values.[33,34] Transmission electron microscopy (TEM) results reveal amorphous, amorphous–crystalline, and crystalline structures for Ti–EG films annealed at 250, 650, and 850 °C, respectively (Figure 1). Si NWs were used as high aspect ratio nanometric templates for Ti–EG MLD film formation. The films formed on NW templates show similar structural characteristics to films formed on planar substrates with highly conformal and uniform formation of the as-prepared films. Thermal anneal results in gradual transition from amorphous film to anatase phase similar to the results with planar substrates, indicating the potential of the MLD method for the uniform coating of high geometric aspect ratio nanoscale structures and thermal anneal compatibility process (Figures 1 d–f). The electron diffraction patterns for Ti–EG films annealed at 650 and 850 °C show lattice planes associated exclusively with the anatase phase, (101), (004), and (200) with *d*- spacing very close to expected values (Supporting Information, Table S2 and Figure S2).[35] In contrast, for TiO_2 films annealed at 650 and 850 °C the brookite and rutile phases are observed in addition to

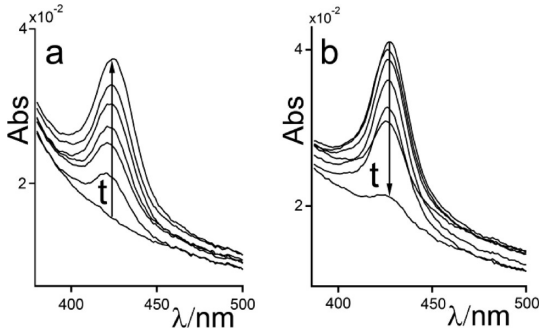

Figure 2. (a) Adsorption and (b) photodegradation of 4OHTPP on Ti−EG film annealed at 650 °C.

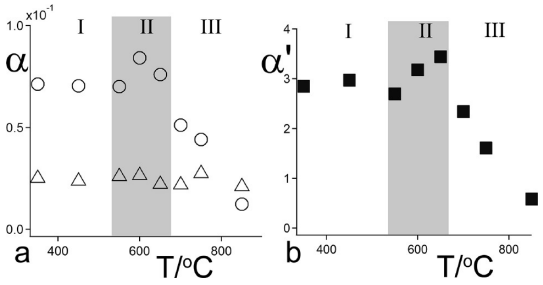

Figure 3. (a) Comparison of 4OHTPP loading to Ti−EG (○), and TiO_2 (Δ) films annealed at different temperatures, where α = A_{425}/A_{261}; A_{425} absorbency corrected for pre-adsorbed film. (b) Relative porphyrin loading (■), calculated by the ratio $\alpha' = \alpha_{Ti-EG}/\alpha_{TiO_2}$.

the main anatase phase. These results suggest that the carbon present in the Ti−EG films suppress the anatase-to-rutile phase transition, in agreement with previous reports.[36,37] The estimated crystallite size from TEM data is in the range 15−20 nm for Ti−EG films annealed at 650 and 850 °C.

To better understand the thermally annealed Ti−EG film properties and photocatalytic activity we performed porphyrin adsorption and photodegradation experiments. Porphyrin molecules are versatile molecular probes for studying molecular interfaces using their unique spectroscopic and structural properties.[38−41] Porphyrin molecules (5,10,15,20-tetrakis(4-hydroxyphenyl)-21*H*,23*H*-porphine, (4OHTPP)) were used as spectroscopic probes to quantify the surface properties as well as photocatalytic activity of the films by measuring the adsorption and photocatalytic decomposition rates of the adsorbed 4OHTPP molecules on the films (Figure 2 and Supporting Information, Figures S3−S6).

Quartz slides were coated with Ti−EG films (40 cycles), annealed at different temperatures, and immersed in 0.08 mM acetonitrile (AN) solution of 4OHTPP for different time intervals until maximal porphyrin loading was reached as indicated by the Soret absorbency (Figure 2a). All porphyrin adsorption studies were carried out in the dark to prevent unintended photodegradation of the surface-adsorbed molecules. Typical UV−vis absorption spectra of Ti−EG film before- and after porphyrin adsorption, and adsorption kinetics are presented in Supporting Information, Figures S3 and S4, respectively. 4OHTPP hydroxyl groups facilitate adsorption of the porphyrin to polar surface groups found in Ti−EG as well as in TiO_2 films from polar aprotic solvents such as acetonitrile. Surface coverage saturation is achieved after ∼2h as reflected by the constant absorbency as a function of time. Control experiments with tetraphenylporphrin (TPP) showed no significant adsorption to the film under the same conditions, thus simple porphyrin aggregation and deposition at the film surface can be ruled out (see Supporting Information, Figure S7). Porphyrin adsorption measurements were performed for Ti−EG and TiO_2 films annealed at various temperatures. Comparison of the 4OHTPP adsorption results for Ti−EG and TiO_2 films for various film anneal temperatures provide valuable insight regarding the role of the sacrificial EG moiety in controlling surface loading of the annealed films. 4OHTPP loading to the films was quantified by the ratio α, defined as A_{425}/A_{261}; where A_{425} is the Soret band absorption corrected for pre-adsorbed film absorbency, and A_{261} is the oxide absorption maxima. We find for Ti−EG films that α is almost constant for annealing temperatures up to ∼600 °C, reach a maximal value at 650 °C, and decrease significantly as the anneal temperature is further increased (Figure 3a, open circles). In contrast, the same analysis performed for 4OHTPP adsorption to TiO_2 films yields an almost constant α value for comparable film thickness and temperature range (Figure 3, open triangles). These results can be explained by considering the effect of thermal anneal on the organic part of the Ti−EG film. As annealing temperature increases above the thermal stability of the EG moiety, a significant portion of the organic part is lost resulting in surface defects and adsorption sites with concomitant gradual formation of crystalline TiO_2 anatase phase embedded within amorphous film as shown by the TEM results (Figure 1). Higher anneal temperature lead to increasing degree of crystallinity, anneal of surface defects, lower degree of amorphous film regions, and overall decrease of adsorption capacity. In addition, for high anneal temperatures, the formation of well-defined, isolated crystallites with exposed underlying substrate is observed in contrast to the observed crystallites embedded within amorphous film for anneal temperatures below 700 °C. Additional support to the TEM results is obtained by the XRD and electron diffraction data (see Supporting Information Table S2 and Figure S2).

Furthermore, a consideration of the ratio, $\alpha' = \alpha_{Ti-EG}/\alpha_{TiO_2}$, representing 4OHTPP loading to Ti−EG relative to TiO_2 films as a function of temperature, reveals three distinct regions (Figure 3b, full rectangles); (I) low-temperature region where porphyrin loading to Ti−EG film is higher compared to TiO_2 with $\alpha' \approx 3$, (II) transition-temperature region, with

increasing porphyrin loading with temperature, and (III) high-temperature region where porphyrin loading is decreasing with temperature for both Ti−EG and TiO_2 films. Comparison of 4OHTPP loading to Ti−EG and TiO_2 films for various film thickness values gave ~5 fold enhancement in favor of the Ti−EG films for the thickness range of 5−40 nm studied here.

XPS analyses performed for annealed Ti−EG films show an increase of the XPS signal intensity for Ti2p and O1s and decrease for the C1s for the same sample before and after thermal anneal at 650 °C, respectively (Supporting Information, Figure S8 and Tables S3−S4). Interestingly, for as-prepared Ti−EG films, the Cl/Ti ratio is 0.3 indicating the presence of chlorine residues. In contrast, for TiO_2 films chlorine residue could not be observed pointing at the reactivity difference of EG compared with water at the deposition temperature (100 °C) and possible steric limitation for EG to react with all $TiCl_4$ species at the surface or entrapped surface reaction products (HCl).[42−44] In addition, XPS data indicate changes of the film composition with O/Ti, and C/Ti atomic ratios of 2.5 and 1.3 for the as-prepared Ti−EG film prior to thermal anneal, and O/Ti and C/Ti atomic ratios of 2.0 and 0.3, respectively, after thermal anneal at 650 °C. These results suggest that during the thermal anneal process a significant portion of the organic component decomposes as indicated by substantial carbon content loss, while mainly Ti-, and O-frameworks compose the annealed film structure. The substantial retention of the Ti and O framework is further indicated by the increase in Ti2p and O1s signal intensity with concomitant decrease in the C1s signal intensity. In addition, both ellipsometry and TEM measurements show substantial decrease in the film thickness following thermal annealing. The atomic ratio of 0.1−0.3 for C/Ti is observed for Ti−EG films annealed at 650 and 850 °C, suggesting incorporation of carbon in the annealed films. However, the presence of carbon in the annealed films did not result in a red shift of the absorption edge of Ti−EG films or increased absorbency in the visible light region as previously reported C-doped TiO_2 systems.[45,46] The complete surface reaction of $TiCl_4$ with EG yielded the expected C/Ti ratio of 4/1 for the as-prepared films. The low C/Ti ratio obtained by XPS analysis for Ti−EG films suggests an incomplete surface reaction, which is also supported by the presence of the Cl peak obtained. In addition, we observe partial hydrolysis of the preannealed Ti−EG films when it is transferred in ambient air by moisture observed by TEM (Supporting Information, Figure S9) and ellipsometry (not shown). Hydrolysis of Ti−O−EG by ambient water molecules may result in Ti−O−Ti species that is expected to show reduced film thickness and carbon content. To quantify the photocatalytic activity of the films we define τ, as the illumination time (365 nm light) required for bleaching half of the adsorbed 4OHTPP measured by the Soret band maxima, λ_{max} = 425 nm, (Figure 4).

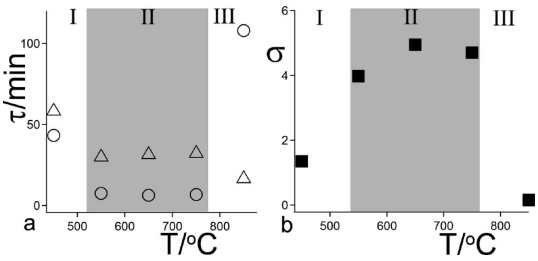

Figure 4. (a) Illumination time, τ, required to deplete half the 4OHTPP absorbency at λ = 425 nm for Ti−EG films (○) and TiO_2 films (△) vs anneal temperature; (b) normalized half depletion times, $\sigma = \tau TiO_2/\tau$Ti−EG (■).

We define the additional parameter, $\sigma = \tau_{TiO_2}/\tau_{Ti-EG}$, as the normalized half depletion times reflecting the photodegradation activity of Ti−EG relative to TiO_2 films toward adsorbed 4OHTPP molecules. A typical Soret band intensity loss indicating 4OHTPP decomposition upon illumination with 365 nm light for Ti−EG film annealed at 650 °C is depicted in Figure 2b.

We find a maximal σ value for anneal temperature of 650 °C, corresponding to ~5 fold higher activity of the Ti−EG film as compared to TiO_2. We find that the photocatalytic activity of annealed Ti−EG films increases in a sharp transition for temperatures above 500 °C reaching almost constant τ value for the temperature range of 550−750 °C (Figure 4 region II). Remarkably, the photocatalytic activity of the Ti−EG films measured by the parameters τ and σ presented in Figure 4 and the TEM imaging and electron diffraction results presented in Figure 1a−f, and Supporting Information, Figure S2 reveal that the film photocatalytic activity and structural characteristics correspond to the three distinct states, similar to our findings from the 4OHTPP loading experiments. Overall, the combined results can be assigned to three anneal temperature regions of the films: (I) amorphous state, intermediate dye loading, low photocatalytic activity, (II) intermediate film state with both crystalline and amorphous regions, high dye loading, high catalytic activity, and (III) highly crystalline film with low dye loading and low photocatalytic activity. As indicated, diffraction data for Ti−EG films annealed at 650 and 850 °C (film states II and III) correspond to the anatase crystalline phase, thus the enhanced photocatalytic activity is not due to variations of the crystalline phase, but rather to the intermediate film state combining accessible adsorption sites and photocatalytic active crystalline regions. Namely, the photocatalytic activity is enhanced by the crystalline regions embedded within amorphous film and capacity of the film volume to interact with the adsorbed molecules. This intermediate state of the film structure is key for enhancing the photocatalytic activity and is made accessible *via* the unique characteristics of the MLD and controllable

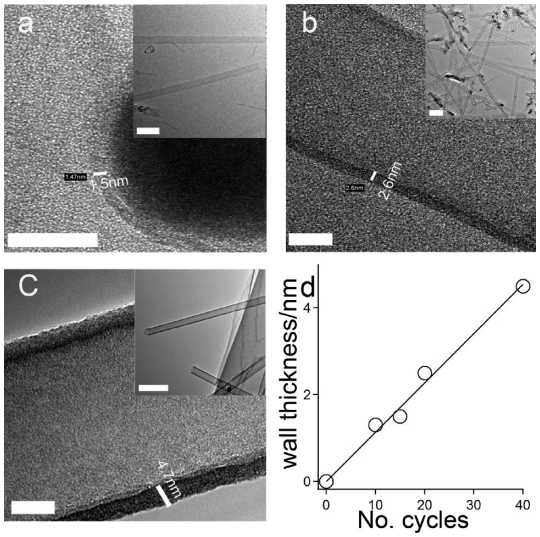

Figure 5. TEM images for Ti—EG NTs formed using sacrificial Ge oxide NWs (a—c). Controllable nanotube wall thickness vs MLD cycle number (d). Scale bars 10 nm (a—c); inset, 200 nm.

anneal process. The photocatalytic activity toward photodegradation of Ti—EG films adsorbed with 4OHTPP was studied under N_2 atmosphere with no significant change in the activity, pointing at direct hole oxidation of the adsorbed molecules and excluding the contribution of reactive oxygen species such as OH or superoxide radicals in the process. In addition to the study of photocatalytic degradation of adsorbed porphyrin molecules, the photocatalytic activity of annealed Ti—EG films immersed in methylene blue (MB) aqueous solution were studied showing activity and stability under working conditions (Supporting Information, Figure S10).

Porphyrin Loading and Photodegradation Studies Using Ti—EG Nanotubes. Ti—EG nanotubes (Ti—EG NTs) were prepared by MLD film formation on sacrificial Ge oxide NWs scaffold and subsequent etch. Oxidized Ge NWs were coated with Ti—EG films and annealed at 350 °C. Next, the Ge oxide core was etched to yield Ti—EG NTs under mild etch conditions with 2—10 min etch suffice for dissolution of the Ge oxide core. In sharp contrast, TiO_2 NTs prepared under similar conditions required several hours of etch to remove the Ge oxide core. This result demonstrates the permeability of the Ti—EG film obtained by the MLD process toward etch solution in contrast to the pinhole-free, nonpermeable TiO_2 film obtained by the ALD process, as expected. The Ti—EG NTs sustain structural integrity upon thermal annealing of 650 °C required for photocatalytic activity. XRD results show the formation of anatase phase exclusively, similar to the results obtained for Ti—EG films. XPS data show minor traces of GeO_2 (not shown).

The photocatalytic activity and surface properties of Ti—EG NTs were studied using 4OHTPP loading experiments. The analysis of these experiments demonstrate

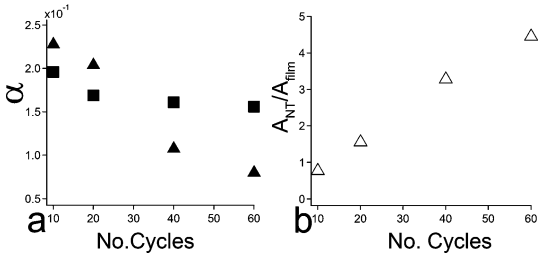

Figure 6. (a) Comparison of 4OHTPP loading to Ti—EG films (▲), and Ti—EG NTs (■) annealed at 650 °C, where α = A_{425}/A_{261}; A_{425} absorbency corrected for preadsorbed film. (b) 4OHTPP loading ratios for Ti—EG NTs compared to Ti—EG films (Δ).

the effect of nanoscale tube morphology compared to planar Ti—EG films. The 4OHTPP loading, α, remain constant for Ti—EG NTs as the tube wall thickness increases (Figure 6a). In contrast, Ti—EG planar films show monotonic decrease of α with film thickness. This result indicates that 4OHTPP loading increases proportionally to the Ti—EG tube wall thickness, demonstrating volume adsorption of the dye, whereas planar Ti—EG films mainly involve surface adsorption. Hence the NT structure avoids structural collapse of the film upon annealing and yield volume adsorption. This leads to higher 4OHTPP loading ratio of Ti—EG NTs compared to Ti—EG films that increase with MLD cycles as presented in Figure 6b. 4OHTPP loading ratios of up to ~5 times were achieved for Ti—EG NTs compared to Ti—EG films. Notably, the half time (τ) measured for 4OHTPP degradation is similar for both NTs and Ti—EG films (Supporting Information, Figure S11), thus the intrinsic photocatalytic properties are similar for both systems.

CONCLUSION

In summary, the formation of photocatalytic thin films showing an amorphous and crystalline hybrid state was demonstrated using the MLD process with $TiCl_4$ and EG precursors. Film formation process is highly controlled with linear film thickness increase per MLD cycle for the temperature range of 100—120 °C studied here. The Ti—EG MLD process yielded highly conformal films on macroscopic substrates as well as on high aspect ratio nanometric structures. Optimization of thermal anneal conditions resulted in substantial decomposition of the film's organic component, crystallite formation, and retention of an amorphous framework that allow for molecular diffusion and adsorption as was demonstrated with porphyrin adsorption experiments. Notably, the intermediate amorphous—crystalline film structure is valuable for designing photocatalytic films. A comparison of Ti—EG films and nanotube morphologies demonstrated increased dye loading capacity of the nanotube structures with linear dye loading increase with wall thickness and similar photocatalytic degradation rates.

Collectively, our results demonstrate the feasibility and high potential of the MLD process to form nanometric hybrid structures with high photocatalytic activity. Additional study is in progress for a better understanding of the the role of annealed film stoichiometry and extending the range of aliphatic diols studied. The approach presented here may be extended to additional metal oxides such as WO_3, NiO, and V_2O_5 for improved oxide catalytic and optoelectronic properties.

MATERIALS AND METHODS

MLD Process. Ti—EG films were prepared using $TiCl_4$ (Acros, 99.9%) and ethylene glycol (Aldrich, > 99%). Ultrapure water (>18MΩ, ELGA purification system) was used for the ALD of TiO_2. Ultrahigh purity Ar gas was used as the carrier gas in the viscous flow reactor and for purge between reactant exposures. MLD films were prepared by dosing the reactant precursors into Ar carrier gas. The duration of precursor dosing was controlled using computer controlled pneumatic valves. A steady state pressure of 2.1×10^{-1} mBar was maintained during the process. For the MLD process the water and EG precursor chamber temperature was set to 40 and 80 °C, respectively. Sample reaction temperature was set to 100, 110, and 120 °C for various processes (see results in Supporting Information, Table S1). The films were prepared on various substrates such as SiO_2/Si wafers, quartz slides, and 40 nm SiO_2 membranes for TEM measurements. Prior to film formation the substrates were cleaned using oxygen plasma for 1 min, 60 W RF power. Unless otherwise mentioned the number of cycles performed was set to 40 cycles for Ti—EG and 220 cycles for TiO_2 films with film thickness of ~16 nm for both. Films were thermally annealed at the different specified temperature for 30 min. For thermal anneal of the films, the oven temperature is equilibrated to the desired temperature prior to sample loading to avoid kinetic effects of temperature ramp rate.

Porphyrin Adsorption and Photocatalytic Degradation Measurements. 5,10,15,20-Tetrakis(4-hydroxyphenyl)-21*H*,23*H*-porphine (4OHTPP) was obtained from Aldrich and used as received. Acetonitrile solutions of 4OHTPP and meso-tetraphenylporphine (TPP) (Strem Chemicals) were prepared and used for adsorption studies as spectroscopic markers. Absorption spectroscopy was performed using a Perkin-Elmer Lambda 1050 spectrophotometer using a custom built slide holder. Ti—EG or TiO_2 films formed on quartz slides were annealed at various temperatures. 4OHTPP adsorption to the films was measured by immersion of the Ti—EG or TiO_2 quartz-coated slides in the 4OHTPP solution for different time intervals until maximal 4OHTPP loading was reached as indicated by the Soret absorbency. All 4OHTPP adsorption studies were carried out in the dark to prevent unintended photodegradation of the surface-adsorbed molecules. For measuring the photocatalytic degradation of 4OHTPP on Ti—EG or TiO_2 films the coated quartz slides were immersed in the 4OHTPP solution for 2 h, rinsed three times with acetonitrile, and dried under N_2 stream in the dark. Then, the dry films were subjected to a 365 nm light source for different time intervals and measurement of the absorption spectra corresponding for each time interval.

Nanowire Growth. Si NWs were grown in a custom built CVD system using a vapor—liquid—solid mechanism. The NW growth process consisted of 440 °C temperature, 35 Torr pressure, 10 min duration, 50 sccm H_2, and 2 sccm SiH_4 gas flow. SiO_2 membranes (40 nm thick) were used as substrates (Ted Pella, Inc.) for NW CVD growth and direct TEM imaging without further sample preparation required. For direct SiO_2/Si NW growth on the membranes a drop of poly-L-lysine solution, 0.1% (w/v) in H_2O (Sigma) was placed on the membrane for 5 min. The membrane was then thoroughly rinsed with DI water and dried over a N_2 stream. Then a drop containing 30 nm of Au nanoparticle solution (Ted Pella, Inc.) was placed on the membrane for 2 min. Again, the membrane was then thoroughly rinsed with DI water and dried over a N_2 stream.

Similarly, Ge NWs were prepared with process parameters set to 245 °C, 45 Torr pressure, 10 min duration, 10 sccm H_2, and 30 sccm GeH_4 gas flow.

Preparation of Ti—EG Nanotubes. Ge NWs were thermally oxidized at 500 °C for 1 h and used as templates for the Ti—EG MLD process. Oxidized Ge NWs were coated with Ti—EG films, preannealed at 350 °C for 30 min, and etched using 0.4% HCl/H_2O_2 (V/V) solution for different time intervals followed by rinsing with DI water. The resulting nanotubes were annealed at the desired final temperature for 30 min.

Characterization Techniques. TEM measurements were performed using FEI Tecnai F20-G^2 system with EFTEM (GATAN GIF 2001).

X-ray photoelectron spectroscopy (XPS) data were collected with a Kratos Axis Ultra X-ray photoelectron spectrometer. Spectra were acquired with monochromatic Al(Kα) radiation. Spectroscopic ellipsometry measurements were performed using a VB-200 spectroscopic ellipsometer (Woolam Co.).

Conflict of Interest: The authors declare no competing financial interest.

Acknowledgment. We thank Dr. Inna Popov for assistance in TEM measurements, Dr. Vitaly Gutkin for XPS analysis. This work was partially funded by the Israel Science Foundation (ISF) under Grant (690/09) and by a starting grant from the European Research Council (ERC) under the European Community's Seventh Framework Programme Grant Agreement No. 259312.

Supporting Information Available: Experimental procedures, Figures S1—S11, Tables S1—S4. This material is available free of charge *via* the Internet at http://pubs.acs.org.

REFERENCES AND NOTES

1. Leskela, M.; Ritala, M. Atomic Layer Deposition (ALD): From Precursors to Thin Film Structures. *Thin Solid Films* **2002**, *409*, 138–146.
2. George, S. M. Atomic Layer Deposition: An Overview. *Chem. Rev.* **2010**, *110*, 111–131.
3. Knez, M.; Nielsch, K.; Niinistö, L. Synthesis and Surface Engineering of Complex Nanostructures by Atomic Layer Deposition. *Adv. Mater.* **2007**, *119*, 3425–3438.
4. Burtman, V.; Zelichenok, A.; Yitzchaik, S. Organic Quantum-Confined Structures through Molecular Layer Epitaxy. *Angew. Chem., Int. Ed.* **1999**, *38*, 2041–2045.
5. Burtman, V.; Ofir, Y.; Yitzchaik, S. In *Situ* Spectroscopic Ellipsometry Monitoring of Multilayer Growth Dynamics *via* Molecular Layer Epitaxy. *Langmuir* **2001**, *17*, 2137–2142.
6. Shirman, T.; Freeman, D.; Posner, Y. D.; Feldman, I.; Facchett, A.; van der Boom, M. E. Assembly of Crystalline Halogen-Bonded Materials by Physical Vapor Deposition. *J. Am. Chem. Soc.* **2008**, *130*, 8162–8163.
7. George, S. M.; Yoon, B.; Dameron, A. A. Surface Chemistry for Molecular Layer Deposition of Organic and Hybrid Organic—Inorganic Polymers. *Acc. Chem. Res.* **2009**, *42*, 498–508.
8. Dameron, A.; Seghete, A. D.; Burton, B. B.; Davidson, S. D.; Cavanagh, A. S.; Bertrand, J. A.; George, S. M. Molecular Layer Deposition of Alucone Polymer Films Using Trimethylaluminum and Ethylene Glycol. *Chem. Mater.* **2008**, *20*, 3315–3326.
9. Liang, X.; Yu, M.; Li, J.; Jiang, Y.-B.; Weimer, A. W. Ultra-Thin Microporous—Mesoporous Metal Oxide Films Prepared by Molecular Layer Deposition. *Chem. Commun.* **2009**, 7140–7142.
10. Gong, B.; Peng, Q.; Parsons, G. N. Conformal Organic—Inorganic Hybrid Network Polymer Thin Films by Molecular

Layer Deposition Using Trimethylaluminum and Glycidol. *J. Phys. Chem. B* **2011**, *115*, 5930–5938.
11. George, S. M.; Lee, B. H.; Yoon, B.; Abdulagatov, A. I.; Hall, R. A. Metalcones: Hybrid Organic–Inorganic Films Fabricated Using Atomic and Molecular Layer Deposition Techniques. *J. Nanosci. Nanotechnol.* **2011**, *11*, 7948–7955.
12. Peng, Q.; Gong, B.; VanGundy, R. M.; Parsons, G. N. "Zincone" Zinc Oxide- Organic Hybrid Polymer Thin Films Formed by Molecular Layer Deposition. *Chem. Mater.* **2009**, *21*, 820–830.
13. Hwang, Y. J.; Boukai, A.; Yang, P. High Density *n*-Si/*n*-TiO_2 Core/Shell Nanowire Arrays with Enhanced Photoactivity. *Nano Lett.* **2009**, *9*, 410–415.
14. Sander, M. S.; Côté, M. J.; Gu, W.; Kile, B. M.; Tripp, C. P. Template-Assisted Fabrication of Dense, Aligned Arrays of Titania Nanotubes with Well-Controlled Dimensions on Substrates. *Adv. Mater.* **2004**, *16*, 2052–2057.
15. Kasuga, T.; Hiramatsu, M.; Hoson, A.; Sekino, T.; Niihara, K. Formation of TiO_2 Nanotube. *Langmuir* **1998**, *14*, 3160–3163.
16. Hulteen, J. C.; Martin, C. R. A General Template-Based Method for the preparation of Nanomaterials. *J. Mater. Chem.* **1997**, *7*, 1075–1087.
17. Kemell, M.; Pore, V.; Tupala, J.; Ritala, M.; Leskela, M. Atomic Layer Deposition of Nanostructured TiO_2 Photocatalysts *via* Template Approach. *Chem. Mater.* **2007**, *19*, 1816–1820.
18. Gong, B.; Peng, Q.; Jur., J. S.; Devine, C. K.; Lee, K.; Parsons, G. N. Sequential Vapor Infiltration of Metal Oxides into Sacrificial Polyester Fibers: Shape Replication and Controlled Porosity of Microporous/Mesoporous Oxide Monoliths. *Chem. Mater.* **2011**, *23*, 3476–3485.
19. Diebold, U. Surface Science of TiO_2. *Surf. Sci. Rep.* **2003**, *48*, 53–229.
20. Fujishima, A.; Zhang, X.; Tryk, D. A. TiO_2 Photocatalysis and Related Surface Phenomena. *Surf. Sci. Rep.* **2008**, *63*, 515–582.
21. O'Regan, B.; Grätzel, M. A Low Cost Highly Efficient Solar Cell Based on Dye Sensitized Colloidal TiO_2 Films. *Nature* **1991**, *353*, 737.
22. Hagfeldt, A.; Grätzel, M. Molecular Photovoltaics. *Acc. Chem. Res.* **2000**, *33*, 269–277.
23. Kavan, L.; Kalbac, M.; Zukalova, M.; Exnar, I. Lithium Storage in Nanostructured TiO_2 Made by Hydrothermal Growth. *Chem. Mater.* **2004**, *16*, 477–485.
24. Armstrong, A. R.; Armstrong, G.; Canales, J.; Gracia, R.; Bruce, P. G. Lithium Ion Intercalation into TiO_2-B Nanowires. *Adv. Mater.* **2005**, *17*, 862–865.
25. Chen, Y. W; Prange, J. D.; Dühnen, S.; Park, Y; Gunji, M.; Chidsey, C. E. D.; McIntyre, P. C. Atomic Layer-Deposited Tunnel Oxide Stabilizes Silicon Photoanodes for Water Oxidation. *Nat. Mater.* **2011**, *10*, 539–544.
26. Wang, R.; Hashimoto, K.; Fujishima, A.; Chikuni, M.; Kojima, E.; Kitamura, A.; Shimohigoshi, M.; Watanabe, T. Light Induced Amphiphilic Surfaces. *Nature* **1997**, *388*, 431–132.
27. Yue, Y.; Gao Synthesis of Mesoporous TiO_2 with a Crystalline Frame Work. *Chem. Commun.* **2000**, 1755–1756.
28. Crepaldi, E. L.; Soler-Illia, G. J.; de, A. A.; Grosso, D.; Cagnol, F.; Ribot, F.; Sanchez, C. Controlled Formation of Highly Organized Mesoporous Titania Thin Films: From Mesostructured Hybrids to Mesoporous Nanoanatase TiO_2. *J. Am. Chem. Soc.* **2003**, *125*, 9770–9786.
29. Choi, S. Y.; Mamak, M.; Coombs, N.; Chopra, N.; Ozin, G. A. Thermally Stable Two-Dimensional Hexagonal Mesoporous Nanocrystalline Anantase, Meso-nc-TiO_2: Bulk and Crack-free Thin Film Morphologies. *Adv. Funct. Mater.* **2004**, *14*, 335–344.
30. Luo, H.; Wang, C.; Yan, Y. Synthesis of Mesostructured Titania with Controlled Crystalline Framework. *Chem. Mater.* **2003**, *15*, 3841–3846.
31. Chae, S. Y.; Park, M. K.; Lee, S. K.; Kim, T. Y.; Kim, S. K.; Lee, W. I. Preparation of Size-Controlled TiO_2 Nanoparticles and Derivation of Optically Transparent Photocatalytic Films. *Chem. Mater.* **2003**, *15*, 3326–3331.
32. Ye, J.; Liu, W.; Cai, J.; Chen, S.; Zhao, X.; Zhou, H.; Qi, L. Nanoporous Anatase TiO_2 Mesocrystals: Additive-free Synthesis, Remarkable Crystalline-Phase Stability, and Improved Lithium Insertion Behavior. *J. Am. Chem. Soc.* **2011**, *133*, 933–940.
33. Aarik, J.; Aidla, A.; Mandar, H.; Uustare, T. Atomic Layer Deposition of Titanium Dioxide from $TiCl_4$ and H_2O: Investigation of Growth Mechanism. *Appl. Surf. Sci.* **2001**, *172*, 148–158.
34. Aarika, J.; Aidla, A.; Mandar, H.; Uustare, T.; Schuisky, M.; Harsta, A. Atomic Layer Growth of Epitaxial TiO_2 Thin Films from $TiCl_4$ and H_2O on α-Al_2O_3 Substrates. *J. Cryst. Growth* **2002**, *242*, 189–198.
35. Weirich, T. E.; Winterer, M.; Seifried, S.; Mayer, J. Structure of Nanocrystalline Anatase Solved and Refined from Electron Powder Data. *Acta Crystallogr., Sect. A* **2002**, *58*, 308–315.
36. Shanmugam, S.; Gabashvili, A.; Jacob, D. S.; Yu, J. C.; Gedanken, A. Synthesis and Characterization of TiO_2@C Core–Shell Composite Nanoparticles and Evaluation of Their Photocatalytic Activities. *Chem. Mater.* **2006**, *18*, 2275–2282.
37. Inagaki, M.; Kojin, F.; Tryba, B.; Toyoda, M. Carbon-Coated Anatase: The Role of the Carbon Layer for Photocatalytic Performance. *Carbon* **2004**, *43*, 1652–1659.
38. Yerushalmi, R.; Scherz, A; van der Boom, M. Enhancement of Molecular Properties in Thin Films by Controlled Orientation of Molecular Building Blocks. *J. Am. Chem. Soc.* **2004**, *126*, 2700–2701.
39. Gulino, A.; Fragala, I.; Scamporrino, E.; Vitalini, D. Similarities and Differences among Monolayers of a Free Base Porphyrin and Its Copper Complex: Synthesis and Characterization of a Luminescent Copper (II) Porphyrin Monolayer. *J. Phys. Chem. C* **2007**, *111*, 14125–14130.
40. Vesper, B. J; Salaita, K.; Zong, H.; Mirkin, C. A.; Barrett, A. G. M.; Hoffman, B. M. Surface-Bound Porphyrazines: Controlling Reduction Potentials of Self-Assembled Monolayers through Molecular Proximity/Orientation to a Metal Surface. *J. Am. Chem. Soc.* **2004**, *126*, 16653–16658.
41. Gulino, A.; Giuffrida, S.; Mineo, P.; Purrazzo, M.; Scamporrino, E.; Ventimiglia, G.; van der Boom, M. E.; Fragala, I. Photoluminescence of a Covalent Assembled Porphyrin-Based Monolayer: Optical Behavior in the Presence of O_2. *J. Phys. Chem. B.* **2006**, *110*, 16781–16786.
42. Aarik, J.; Aidla, A.; Mandar, H.; Uustare, T. Atomic Layer Deposition of Titanium Dioxide from $TiCl_4$ and H_2O: Investigation of Growth Mechanism. *Appl. Surf. Sci.* **2001**, *172*, 148–158.
43. Tiznado, H.; Zaera, F. Surface Chemistry in the Atomic Layer Deposition of TiN Films from $TiCl_4$ and Ammonia. *J. Phys. Chem. B* **2006**, *110*, 13491–13498.
44. Methaapanon, R.; Bent, F. S. Comparative Study of Titanium Dioxide Atomic Layer Deposition on Silicon Dioxide and Hydrogen-Terminated Silicon. *J. Phys. Chem. C* **2010**, *114*, 10498–10504.
45. Sakthivel, S.; Kisch, H. Daylight Photocatalysis by Carbon-Modified Titanium Dioxide. *Angew. Chem., Int. Ed.* **2003**, *42*, 4908–4911.
46. Zhang, L.; Koka, R. V. A. Study on The Oxidation and Carbon Diffusion of TiC in Alumina–Titanium Carbide Ceramics Using XPS and Raman Spectroscopy. *Mater. Chem. Phys.* **1998**, *57*, 23–32.